Physics – Uspekhi **64** (3) 304 – 316 (2021)

INSTRUMENTS AND METHODS OF INVESTIGATION

PACS numbers: **41.60. – m**, 41.60.Ap, 41.60.Cr

Undulator and free-electron laser radiation with field harmonics and off-axis effects taken into account analytically

K V Zhukovsky

DOI: https://doi.org/10.3367/UFNe.2020.06.038803

Contents

Abstract. We present an analytic description of the generation of undulator radiation (UR) harmonics in a generalized elliptic undulator with field harmonics. The obtained analytic expressions for generalized Bessel and Airy functions describe the UR spectral lines and radiation intensity in the general and particular cases of two-frequency planar and helical undulators and also for other elliptic and planar undulators. We analytically describe the effect of finite electron beam size, beam emittance, off-axis deflection of electrons, electron energy spread, and beam-bending permanent magnetic components. The obtained analytic expressions distinguish the contributions made by each field component and by the beam and undulator parameters to the generation of radiation harmonics. Using an analytic model of single-pass free-electron lasers (FELs), we analyze the power evolution of harmonics in the LCLS, LEUTL, and SACLA FEL experiments. We discuss the effect that the beam and undulator parameters have on the generation of harmonics. It is shown that the strong second harmonics of radiation observed in experiments are caused by the detected beam deviation from the axis by 15 μm over one gain length of 1.5 m in the X-ray LCLS FEL and by the large beam cross section of ∼ 200 μm in the LEUTL FEL. The results of modeling are fully consistent with experiments, which confirms the validity of the presented theoretical description of FEL power and radiation spectral density.

Keywords: undulator, magnetic field, free-electron laser, harmonic generation

K V Zhukovsky
Lomonosov Moscow State University, Faculty of Physics,
Leninskie gory 1, str. 2, 119991 Moscow, Russian Federation
E-mail: zhukovsk@physics.msu.ru

Received 26 December 2019, revised 2 April 2020
Uspekhi Fizicheskikh Nauk **191** (3) 318 – 330 (2021)
Translated by S Alekseev

1. Introduction

Undulator radiation (UR) was first proposed by Ginzburg [1]; the first undulator was constructed by Motz [2], who was also the first to conduct observations of UR. Over the decades that have passed since then, progress in technology has resulted in the appearance of free-electron lasers (FELs), in which, in full accord with Ginsburg's hypothesis, coherent radiation is generated by electrons that are grouped into microbunches less than the radiation wavelength λ_0 in size, separated by a distance equal to the wavelength λ_0. The electron energy E in an undulator is typically high, such that the corresponding relativistic factor is by order of magnitude $\gamma = E/(mc^2) \approx 10^3 - 10^4 \gg 1$, where m is the electron mass and c is the speed of light. This allows obtaining X-ray coherent radiation for investigating processes occurring on the nanoscale [3–10]. We note that coherent radiation in the X-ray range and gamma range can also be generated, besides by FELs, by inverse Compton scattering on electrons and inverse resonance scattering of optical-range laser beam photons by partially ionized ions [11].

The efficient bunching of electrons requires a high quality of the beams and undulators: deviations of the field from an ideally periodic one must be reduced to a minimum; non-periodic components, off-axis deviations of the beam, and energy spread of electrons in the beam must be suppressed. In reality, all these factors are present in undulators to some extent, leading to losses, UR spectrum line broadening, and worsening of the electron bunching, whose efficiency is determined by the conditions on the energy spread $\sigma_e \leqslant \rho/2$ and the emittance $\varepsilon_{x,y} \leqslant \lambda_0/(4\pi)$ (see, e.g., [5, 12]), where ρ is the Pierce parameter of the FEL (see, e.g., [12, 13]) and λ_0 is the radiation wavelength. It must also be taken into account that an ideal harmonic field in undulators has not yet been realized in real devices, because it does satisfy the Maxwell equations off the axis, and also because of the presence of field harmonics. In undulators with permanent magnets, a biharmonic field can be obtained by shimming with ferro-

magnetic materials [14–20]. In some cases, the measured amplitude of field harmonics is as high as $\sim 20-30\%$ of the main field strength [18, 21, 22]. The effect of biharmonic components on the emission of electromagnetic undulators was studied, e.g., in [23, 24]; emission of higher UR harmonics was enhanced compared with the case of a standard undulator [19, 25]. The effect of field harmonics on UR in undulators with permanent magnets and with electromagnets was also studied in [26–29]; it was shown that field harmonics can facilitate the enhanced generation of higher radiation harmonics in FELs, which is advantageous from the standpoint of the possible use of lower-energy electrons to obtain higher-frequency radiation. Besides planar undulators, elliptic undulators are also in use (see, e.g., [25]), as are undulators in which the radiation ellipticity can be varied, as in the APPLE-III undulator for the SwissFEL [30], the Delta undulator [31] for the LCLS (Linac Coherent Light Source) [32], and others. Numerical modeling of the emission from such undulators was done in [33].

We note that in an ideal planar undulator only odd harmonics are emitted on the axis, and in a helical undulator only the main pitch is emitted. The radiation power is typically equal to 1–3% and 0.1% of the main pitch power for the respective $n = 3$ and $n = 5$ FEL harmonics. Even harmonics are also observed in the spectrum of some FELs; their power varies strongly depending on the device and can reach $\sim 0.1\%$ of the main pitch power (see, e.g., [34–37]).

The power of harmonics of both spontaneous and induced UR can be modeled numerically in each particular case using dedicated software. However, numerical computation requires personnel ready to work with that software, computational resources, and the software itself. This can be justified when designing an FEL, but is not necessarily available in the course of investigations or when comparing different devices with each other. In numerical modeling, in addition, it is difficult to reveal the physical reasons for the occurrence of some harmonics in the spectrum. It is therefore relevant to study the generation of harmonics in real devices analytically, taking the parameters of the undulators and beams into account.

In this paper, we theoretically analyze and investigate the behavior of harmonics of spontaneous and induced UR in an undulator with a multicomponent magnetic field, including its harmonics taking all the main losses into account. The analytic relations that we obtain for such an undulator imply limiting cases of planar, helical, and elliptical undulators with the additional periodic and nonperiodic components. We also investigate and quantitatively explain the appearance of even harmonics in some FELs and their measured power.

2. Radiation from a generalized elliptical undulator and its limiting cases

We consider the UR of an elliptical undulator; the radiation of an electron in it can be calculated using the integral radiation

$$\frac{\mathrm{d}^2 I}{\mathrm{d}\omega\,\mathrm{d}\Omega} = \frac{e^2}{4\pi^2 c}\left|\omega\int_{-\infty}^{\infty}\mathrm{d}t\,[\mathbf{n}\times(\mathbf{n}\times\boldsymbol{\beta})]\exp\left[\mathrm{i}\omega\left(t-\frac{\mathbf{nr}}{c}\right)\right]\right|^2, \quad (1)$$

where $\mathbf{n} \cong (\theta\cos\varphi, \theta\sin\varphi, 1-\theta^2)$ is the unit vector in the direction from the charge to the observer, ω is the radiation frequency, $\boldsymbol{\beta}$ is the velocity of the charge, and $\mathbf{r}$ is the radius vector of the charge. Let us consider the magnetic field $\mathbf{H}$ of an elliptical undulator with amplitude H_0, fundamental period λ_u, and multiple periods:

$$\mathbf{H} = H_0\big(\sin(k_\lambda z) + d\sin(pk_\lambda z),\ d_1\sin(hk_\lambda z) + d_2\cos(lk_\lambda z), 0\big),$$
$$k_\lambda = \frac{2\pi}{\lambda_{\mathrm{u},x}}, \quad \lambda_{\mathrm{u},x} \equiv \lambda_\mathrm{u}, \quad h,l,p \in \mathbf{Z}, \quad d,d_1,d_2 \in \mathbf{R}, \quad (2)$$

where Z and R are the respective sets of integer and real numbers. The field harmonics can have an arbitrary intensity in the model. This allows using field (2) to obtain limiting cases of a planar two-frequency undulator and some elliptical undulators (including with field harmonics) that have been investigated previously [39–44]. In the calculations in what follows, we use the method of generalized Bessel functions, which we developed in [43], and a similar formalism developed by other authors in [45–48], where the generation of hard circularly polarized gamma radiation at higher UR harmonics was studied. In [49], the inverse problem was solved of finding the undulator field distribution with linearly polarized radiation on the axis in optimum conditions. The conclusion was that the field of such an undulator is essentially described by the sum of the first and third harmonics, and we use this in choosing the field configuration. Proceeding similarly, we obtain the following expression for the UR intensity in field (2) in the relativistic limit $1/\gamma \ll 1$:

$$\frac{\mathrm{d}^2 I}{\mathrm{d}\omega\,\mathrm{d}\Omega} = \frac{e^2 N^2 k^2}{4\gamma^2 c}\sum_{n=-\infty}^{\infty}\left(\frac{\lambda_\mathrm{u}}{\lambda_n}\right)^2 \mathrm{sinc}^2\left(\frac{\nu_n}{2}\right)\left(\left|f_{n,x}^{1,2}\right|^2 + \left|f_{n,y}^{1,2}\right|^2\right). \quad (3)$$

Here, sinc (...) describes the ideal line shape of the UR spectrum as a function of the undulator detuning parameter $\nu_n = 2\pi nN(\omega/\omega_n - 1)$, where $\omega_n = 2\pi c/\lambda_n$,

$$\lambda_n = \frac{\lambda_\mathrm{u}}{2n\gamma^2}\left[1 + \frac{k^2}{2}\left(1 + \left(\frac{d}{p}\right)^2 + \left(\frac{d_1}{h}\right)^2 + \left(\frac{d_2}{l}\right)^2\right) + (\gamma\theta)^2\right] \quad (4)$$

is the resonance UR length, and $f_{n;x,y}$ are the Bessel coefficients of the corresponding UR polarizations

$$f_{n;x}^1 = \frac{d_1}{h}(J_{n+h}^n + J_{n-h}^n) + \mathrm{i}\,\frac{d_2}{l}(J_{n+l}^n - J_{n-l}^n), \quad (5)$$
$$f_{n;x}^2 = \frac{2}{k}J_n^n\gamma\theta\cos\varphi,$$
$$f_{n;y}^1 = (J_{n+1}^n + J_{n-1}^n) + \frac{d}{p}(J_{n+p}^n + J_{n-p}^n), \quad (6)$$
$$f_{n;y}^2 = \frac{2}{k}J_n^n\gamma\theta\sin\varphi,$$

expressed in terms of the undulator parameter $k = H_0\lambda_{\mathrm{u};x}e/(2\pi mc^2)$, the off-axis deviation angle θ, the azimuthal angle φ, and the generalized Bessel functions

$$J_n^m(\xi_i) = \frac{1}{2\pi}\int_{-\pi}^{\pi}\mathrm{d}\alpha\,\exp\Big[\mathrm{i}\Big(n\alpha + \xi_1\sin(h\alpha) + \xi_2\cos(l\alpha)$$
$$+ \xi_3\sin\alpha + \xi_4\sin(2\alpha) + \xi_5\sin(2h\alpha) + \xi_6\sin(2l\alpha)$$
$$+ \xi_7\cos\big[(l+h)\alpha\big] + \xi_8\cos\big[(l-h)\alpha\big] + \xi_0\sin(p\alpha)$$
$$+ \xi_9\sin\big[(p+1)\alpha\big] + \xi_{10}\sin\big[(p-1)\alpha\big] + \xi_{11}\sin(2p\alpha)\Big)\Big]. \quad (7)$$

They have the indices m, n and depend on the following arguments ξ_i:

$$\xi_4 = \frac{1}{4}\,\frac{mk^2}{1+\dfrac{k^2}{2}\left(1+\left(\dfrac{d}{p}\right)^2+\left(\dfrac{d_1}{h}\right)^2+\left(\dfrac{d_2}{l}\right)^2\right)+\gamma^2\theta^2}\,, \quad (8)$$

$$\xi_0 = \frac{\xi_4 8d}{kp^2}\,\gamma\theta\sin\varphi\,, \quad \xi_1 = \frac{\xi_4 8d_1}{kh^2}\,\gamma\theta\cos\varphi\,,$$
$$\xi_2 = \frac{\xi_4 8d_2}{kl^2}\,\gamma\theta\cos\varphi\,, \quad \xi_3 = \frac{\xi_4 8}{k}\,\gamma\theta\sin\varphi\,, \quad (9)$$

$$\xi_5 = \frac{d_1^2}{h^3}\,\xi_4\,, \quad \xi_6 = -\frac{d_2^2}{l^3}\,\xi_4\,, \quad \xi_{11} = \frac{d^2}{p^3}\,\xi_4\,, \quad (10)$$

$$\xi_7 = \frac{4d_1d_2}{hl(l+h)}\,\xi_4\,, \quad \xi_8 = \frac{4d_1d_2}{hl(l-h)}\,\xi_4\,,$$

$$\xi_9 = \frac{4d}{p(p+1)}\,\xi_4\,, \quad \xi_{10} = \frac{4d}{p(p-1)}\,\xi_4\,. \quad (11)$$

On the axis, $\theta = 0$ and the expressions are greatly simplified, but the dependence on the angle θ is of fundamental importance, because it allows tracing the origin of the even UR harmonics. Analytic expressions (3)–(11) give the dependence of the UR intensity on the undulator parameters and angles in the most general form and allow finding the contribution of each parameter to the generation of UR harmonics.

We consider several limiting cases of field (2). In the field with a sin−sin configuration,

$$\mathbf{H} = H_0\big(d_1\sin(hk_\lambda z), \sin(k_\lambda z), 0\big)\,,$$
$$k_\lambda = \frac{2\pi}{\lambda_\mathrm{u}}\,, \quad h\in\mathbf{Z}\,, \quad d_1, h = \mathrm{const}\,, \quad (12)$$

in accordance with [45–48], we obtain the Bessel coefficients

$$f_{n;\,x}^{1;\,\sin\sin} = (J_{n+1}^n + J_{n-1}^n)\,, \quad f_{n;\,x}^{2;\,\sin\sin} = \frac{2}{k}\,J_n^n\gamma\theta\sin\varphi\,,$$
$$f_{n;\,y}^{1;\,\sin\sin} = \frac{d_1}{h}(J_{n+h}^n + J_{n-h}^n)\,, \quad f_{n;\,y}^{2;\,\sin\sin} = \frac{2}{k}\,J_n^n\gamma\theta\cos\varphi\,. \quad (13)$$

The angular dependence on θ and φ is taken into account in the arguments ξ_4, ξ_1, ξ_3, and ξ_5 of Bessel functions (7); $d = d_2 = 0$ in the corresponding expressions. Skipping the trivial case $h = 1$ in (13), in accordance with the suggestion in [49], we consider the case $h = 3$: $\mathbf{H} = H_0(d_1\sin[2\pi z/(\lambda_\mathrm{u}/3)], \sin(2\pi z/\lambda_\mathrm{u}), 0)$. For x-polarized radiation, we have the Bessel coefficient $f_{n;\,x}$ that is practically independent of d; for y-polarized radiation, the coefficient $f_{3;\,y}$ turns out to be the largest, $f_{5;\,y}$ is slightly less, and $f_{1;\,y}$ is much less than $f_{3,\,5;\,y} \approx 0.1-0.3$ for $|d| \approx 0.5-1$.

We thus see that in asymmetric field (12), UR has stronger higher harmonics in the y-polarization, with the Bessel coefficients being larger than those for the main pitch: $f_{3,\,5;\,y} \gg f_{1;\,y}$. The case $h = 5$ and other higher field harmonics, in full agreement with [49], do not make a significant contribution to UR. We note that the choice $d_1 = 1$ in (12) allows obtaining a planar undulator with the field amplitude $\sqrt{2}H_0$; the corresponding Bessel coefficients are given by expressions (13).

In the limiting case of an elliptical magnetic field with the sin−cos configuration,

$$\mathbf{H} = H_0\big(d_2\cos(lk_\lambda z), \sin(k_\lambda z), 0\big)\,,$$
$$k_\lambda = \frac{2\pi}{\lambda_\mathrm{u}}\,, \quad l\in\mathbf{Z}\,, \quad l, d_2 = \mathrm{const}\,, \quad (14)$$

we obtain Bessel coefficients (7) with $d = d_1 = 0$ in the remaining arguments ξ_4, ξ_2, ξ_3, and ξ_6; for x- and y-polarizations, we then obtain the expressions

$$f_{n;\,x}^{1;\,\sin\cos} = J_{n+1}^n + J_{n-1}^n\,, \quad f_{n;\,x}^{2;\,\sin\cos} = \frac{2}{k}\,J_n^n\gamma\theta\sin\varphi\,,$$
$$f_{n;\,y}^{1;\,\sin\cos} = \frac{d_2}{l}(J_{n+l}^n - J_{n-l}^n)\,, \quad f_{n;\,y}^{2;\,\sin\cos} = \frac{2}{k}\,J_n^n\gamma\theta\cos\varphi\,. \quad (15)$$

At $l = 3$, with the third field harmonic, we obtain the coefficients $f_{n;\,x,\,y}$ and the behavior of harmonics similar to those in the case of a sin−sin field. At $l = 1$, we have identical undulator periods, and for $d \equiv d_2 = \pm 1$ we obtain the known helical undulator.

A planar undulator with the field harmonics

$$\mathbf{H} = H_0\left(0, \sin\frac{2\pi z}{\lambda_\mathrm{u}} + d\sin\frac{2\pi p z}{\lambda_\mathrm{u}}\,, 0\right),$$
$$p\in\mathbf{Z}\,, \quad d, p = \mathrm{const}\,, \quad (16)$$

where ξ_4, ξ_0, ξ_3, ξ_{11}, ξ_{10}, and ξ_9 are the remaining arguments (7) and $d_1 = d_2 = 0$, was investigated in detail, for example, in [50]. The corresponding Bessel coefficients are

$$f_{n;\,x}^{1;\,\sin+\sin} = (J_{n+1}^n + J_{n-1}^n) + \frac{d}{p}(J_{n+p}^n + J_{n-p}^n)\,,$$
$$f_{n;\,x}^{2;\,\sin+\sin} = \frac{2}{k}\,J_n^n\gamma\theta\sin\varphi\,, \quad (17)$$
$$f_{n;\,y}^{1;\,\sin+\sin} = f_{n;\,y}^{2;\,\sin+\sin} = \frac{2}{k}\,J_n^n\gamma\theta\cos\varphi\,.$$

In addition to the analysis performed in [50], we note that the main conclusion in that case is that, for $d > 0$, higher UR harmonics are amplified and the main pitch intensity becomes somewhat weaker for $k > 1.5$ and $p = 3$, thus confirming the conclusion in [49] regarding the decisive effect of the third field harmonic. Other field harmonics have no decisive impact on the generation of UR harmonics. The main effect of the higher UR harmonic amplification is achieved for $d \approx 0.5$ and, naturally, is increased as the undulator parameter k increases (see [50]) (Fig. 1).

In the helical undulator field

$$\mathbf{H} = H_0\big(\sin(k_\lambda z) - d\sin(hk_\lambda z), \cos(k_\lambda z) + d\cos(hk_\lambda z), 0\big)\,, \quad (18)$$

a third harmonic ($h = 3$) has been detected with amplitude $d \approx 0.08$ [25]. For field (18), we obtain the Bessel coefficients [50]

$$f_{n;\,x}^{1;\,\mathrm{asym}} = \mathrm{i}(J_{n+1}^n - J_{n-1}^n) + \mathrm{i}\,\frac{d}{h}(J_{n+h}^n - J_{n-h}^n)\,,$$
$$f_{n;\,x}^{2;\,\mathrm{asym}} = \frac{2}{k}\,J_n^n\gamma\theta\cos\varphi\,, \quad (19)$$

$$f_{n;\,y}^{1;\,\mathrm{asym}} = -(J_{n+1}^n + J_{n-1}^n) + \frac{d}{h}(J_{n+h}^n + J_{n-h}^n)\,,$$
$$f_{n;\,y}^{2;\,\mathrm{asym}} = \frac{2}{k}\,J_n^n\gamma\theta\sin\varphi\,, \quad (20)$$

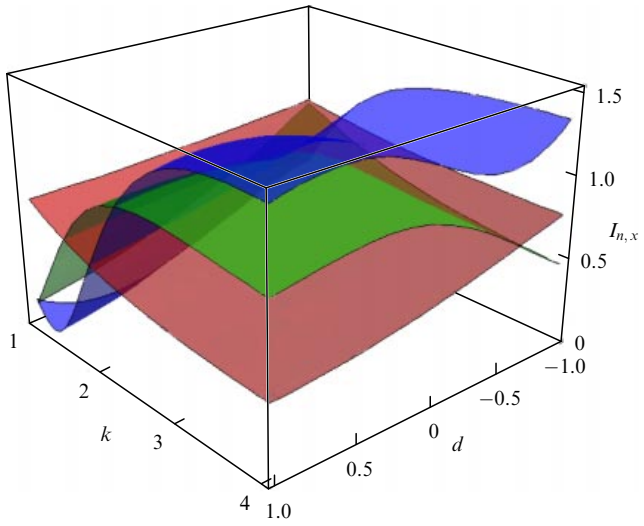

Figure 1. (Color online.) Dimensionless intensity $I_{n;x}$ of the $n = 1, 3, 5$ UR harmonics in a planar undulator with the third field harmonic (16), $p = 3$, $1 < k < 4$. Surfaces correspond to the UR harmonics: the brick red one to $n = 1$, green to $n = 3$, and blue to $n = 5$.

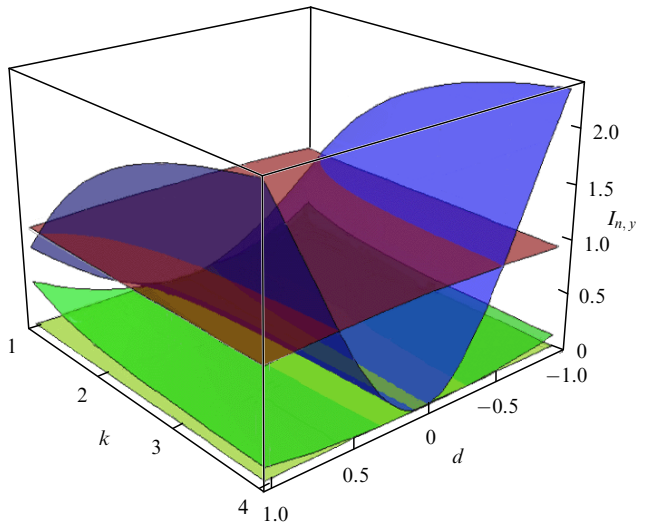

Figure 2. (Color online.) Dimensionless intensity $I_{n;x,y}$ of the $n = 1, 2, 3, 5$ UR harmonics in undulator field (18) with $h = 3$ and $1 < k < 4$, $-1 < d < 1$. Surfaces correspond to the UR harmonics: the brick red one to $n = 1$, yellow to $n = 2$, green to $n = 3$, and blue to $n = 5$.

where d and h correspond to field (18), the superscript asym in (19) and (20) denotes the asymmetric field configuration (18) in the corresponding undulator, and the generalized Bessel functions are [50]

$$J_n^m = \int_{-\pi}^{\pi} \exp\left\{\mathrm{i}\Big(n\alpha + \xi_1 \cos\alpha + \xi_2 \cos(h\alpha) - \xi_3 \sin\alpha + \xi_4 \sin(h\alpha) - \xi_5 \sin\big[(h+1)\alpha\big]\Big)\right\} \frac{\mathrm{d}\alpha}{2\pi}\,, \tag{21}$$

with their arguments expressed as

$$\xi_0 = \frac{2mk}{1 + k^2\big[1 + (d/h)^2\big] + \gamma^2\theta^2}\,, \tag{22}$$

$$\xi_1 = \xi_0\gamma\theta\cos\varphi\,, \quad \xi_2 = \frac{d}{h^2}\,\xi_1\,, \quad \xi_3 = \xi_1\tan\varphi\,, \quad \xi_4 = \frac{d}{h^2}\,\xi_1\tan\varphi\,, \quad \xi_5 = \xi_0\,\frac{kd}{h(h+1)}\,. \tag{23}$$

It was shown in [50] that the fifth UR harmonic in field (18) is already apparent at $d \sim 0.1$ and becomes dominant in the spectrum of spontaneous UR for $d > 0.5$. This is illustrated in Fig. 2, which complements the analysis in [50].

However, in the spectrum of FELs with self-amplified spontaneous emission (SASE), the fifth radiation harmonic of undulator field (18) is only slightly stronger than the original noise of the electron bunch. Although the power of the fifth harmonic of FEL emission is greater than the third harmonic power, the fifth FEL harmonic remains four orders of magnitude weaker than the main FEL pitch, even for the field harmonic amplitude $d \sim 0.3-0.5$ [50, 51].

3. Corrections to undulator radiation due to the energy spread and off-axis effects

In real devices, it must be taken into account that each electron in the beam has its own energy and direction of motion, and its trajectory can run at a distance from the undulator axis, where the magnetic field differs from the simplest model field of form (2), (12), (14), (16), (18), etc. The UR on the undulator axis is discussed most frequently, but, even in that case, the energy spread of electrons in the beam must be taken into account, which is done by using the convolution in the expression for the radiation intensity

$$\int_{-\infty}^{\infty} \frac{\mathrm{d}^2 I(v_n + 4\pi n N\varepsilon, \theta)}{\mathrm{d}\omega\,\mathrm{d}\Omega\,\sqrt{2\pi}\sigma_\mathrm{e}} \exp\left(-\frac{\varepsilon^2}{2\sigma_\mathrm{e}^2}\right) \mathrm{d}\varepsilon\,.$$

In addition, the emittance and size of the beam must be taken into account, together with the possible effect of nonperiodic field components, which result in somewhat shifting the UR spectrum down in frequency and changing the UR line shape. Taking these factors into account in FELs, together with the fact that the electron–photon interaction at higher UR harmonics is more sensitive to losses, is a complicated task. Typically, this is done using a software code that solves the entire set of equations of motion for electrons interacting with the wave field in one- or three-dimensional cases. This software is written for a fixed configuration of the undulator field, and working with it requires a qualified staff. Adapting a given software to an arbitrary undulator field is impossible; its modification to another field configuration, different from the specified one, is done by software developers. On the other hand, analytic tools for describing the operation of FELs, and in particular a phenomenological FEL model in its most recent version [52], allow for a good description of the evolution of the power of FEL harmonics for virtually any undulator, but require an exact analytic expression for all losses.

3.1 Effect of a permanent magnetic field

The effect of nonperiodic magnetic components in undulators should be brought to a minimum [53], because they lead to the broadening of the UR sinc $(v_n/2)$ spectrum lines. For this, the integrals of the field must be carefully evaluated and minimized [44, 45], with the effect of external fields screened or compensated. Some numerical estimates, for example, for the Sibir-2 device, are given in [54, 55]. The permanent field essentially leads to a drift of the electron away from the

undulator axis and the appearance of a field-induced bend angle θ_H. On the axis, the UR user thus sees the radiation of an electron at the induced angle

$$\theta_H = \frac{2\pi}{\sqrt{3}}\,\frac{k}{\gamma}\,N(\kappa^2+\rho^2)^{1/2} \tag{24}$$

due to the transverse permanent components $H_x = H_0\rho$ and $H_y = H_0\kappa$. These lead to the appearance of additional nonperiodic terms in the exponent in the radiation integral, which in turn result in the UR spectrum line shape being given not by the known function $\operatorname{sinc}(v_n/2)$ but by the generalized Airy function written in integral form

$$S(v_n,\eta,\beta) \equiv \int_0^1 \mathrm{d}\tau\,\exp\left[\mathrm{i}(v_n\tau+\eta\tau^2+\beta\tau^3)\right]. \tag{25}$$

The angles θ and φ are involved in the arguments of the special function $S(v_n,\beta,\eta)$

$$\eta = \frac{4\pi^2N^2nk\gamma\theta}{1+k^2/2}\,(\kappa\cos\varphi-\rho\sin\varphi), \tag{26}$$

$$\beta = (2\pi nN+v_n)\,\frac{(\gamma\theta_H)^2}{1+k^2/2} \cong 2\pi nN\,\frac{(\gamma\theta_H)^2}{1+k^2/2}. \tag{27}$$

The UR intensity of a planar undulator can then be expressed as

$$\frac{\mathrm{d}^2I}{\mathrm{d}\omega\,\mathrm{d}\Omega} \cong \frac{e^2N^2\gamma^2k^2}{c(1+k^2/2)^2}\sum_{n=-\infty}^{\infty} n^2\left[S^2(v_n,\eta,\beta)(J_{n+1}^n+J_{n-1}^n)^2 + \left(\frac{2}{k}\,\gamma\theta_H\sqrt{3}\,\frac{\partial S}{\partial v_n}\,J_n^n\right)^2\right]. \tag{28}$$

We note that even UR harmonics on the undulator axis that are due to the permanent field, i.e., the second term in square brackets in (28), are described by the factor $(2/k)\gamma\theta_H\sqrt{3}\,\partial S/\partial v_n$, whence we see that the effect produced by the field is accumulated along the undulator length $L = \lambda_u N$ in θ_H. In the ideal case $\theta_H = 0$, the second term in (28), which corresponds to even UR harmonics on the axis, also vanishes, and $S(v_n,\beta,\eta)$ reduces to $\operatorname{sinc}(v_n/2)$:

$$S(v_n,0,0) = \exp\frac{\mathrm{i}v_n}{2}\,\operatorname{sinc}\frac{v_n}{2}. \tag{29}$$

For multiperiodic undulator fields (2), (12), (14), (16), (18), and others, the structure of expression (28) is preserved; instead of $\operatorname{sinc}(v_n/2)$ in (3), the function S defines a spectrum line of odd harmonics with the corresponding Bessel coefficients $f_{n;\,x,y}^{1,2}$ given in (5), (6), (13), (15), and (17), and the even harmonics on the axis are given by generalized Bessel functions (7) with the coefficients $(2/k)\gamma\theta_H\sqrt{3}\,\partial S/\partial v_n$ (see (28)). For simpler field configurations, the corresponding expressions for $f_{n;\,x,y}^{1,2}$ and $J_n^m(\xi_i)$ are simplified (see Section 2).

We briefly discuss the main properties of generalized Airy functions (25). They are related to the generalized Hermite polynomials in three variables,

$$S(x,y,z) = \sum_{n=0}^{\infty}\frac{\mathrm{i}^nH_n(x,-\mathrm{i}y,-z)}{(n+1)!}. \tag{30}$$

The Hermite polynomials $H_n(x,y,z)$ can be expressed through the sums of two-variate Hermite polynomials $H_n(x,y)$:

$$H_n(x,y,z) = n!\sum_{r=0}^{[n/3]}\frac{z^{n-3r}}{(n-3r)!\,r!}\,H_n(x,y), \tag{31}$$

where [56]

$$H_n(x,y) = n!\sum_{r=0}^{[n/2]}\frac{x^{n-2r}y^r}{(n-2r)!\,r!} \tag{32}$$

can be expressed through the standard Hermite polynomials as

$$H_n(x,y) = (-\mathrm{i})^n y^{n/2}H_n\left(\frac{\mathrm{i}x}{2\sqrt{y}}\right) = \mathrm{i}^n(2y)^{n/2}\,\mathrm{He}_n\left(\frac{x}{\mathrm{i}\sqrt{2y}}\right). \tag{33}$$

The generating exponentials for the Hermite polynomials $H_n(x,y)$ and $H_n(x,y,z)$ are

$$\exp(xt+yt^2) = \sum_{n=0}^{\infty}\frac{t^n}{n!}\,H_n(x,y), \qquad \exp(xt+yt^2+zt^3) = \sum_{n=0}^{\infty}\frac{t^n}{n!}\,H_n(x,y,z). \tag{34}$$

The generalized two- and three-variate Hermite polynomials $H_n(x,y)$ and $H_n(x,y,z)$ can be represented in operator form as the result of acting with exponential differential operators of the respective second and third order on monomials:

$$H_n(x,y) = \exp(y\partial_x^2)x^n, \quad H_n(x,y,z) = \exp(y\partial_x^2+z\partial_x^3)x^n. \tag{35}$$

These operator definitions reveal a nonobvious relation between apparently unrelated mathematical objects and allow a more profound understanding of their physical meaning. For the generalized Airy function $S(x,y,z)$, we obtain the following operator relation to the function $\operatorname{sinc}x$ of the UR spectrum line:

$$\begin{aligned} S(x,y,z) &\equiv \int_0^1 \mathrm{d}\tau\,\exp\left[\mathrm{i}(x\tau+y\tau^2+z\tau^3)\right] \\ &= \exp(-\mathrm{i}y\partial_x^2-z\partial_x^3)\int_0^1\exp(\mathrm{i}x\tau)\,\mathrm{d}\tau \\ &= \exp(-\mathrm{i}y\partial_x^2-z\partial_x^3)\left[\frac{\sin x/2}{x/2}\exp\left(\mathrm{i}\,\frac{x}{2}\right)\right]. \end{aligned} \tag{36}$$

On the undulator axis, $S(x,y,z)$ in (25) is simplified to

$$\begin{aligned} S(x,y,z)\big|_{\text{on axis}} = S(x,z) &= \int_0^1\exp\left[\mathrm{i}(x\tau+z\tau^3)\right]\mathrm{d}\tau \\ &= \sum_{m=0}^{\infty}\frac{\mathrm{i}^mH_m(x,-z)}{(m+1)!}. \end{aligned} \tag{37}$$

The modified shape of the spectrum lines is determined by the behavior of the functions S and $\partial S/\partial v_n$. For odd harmonics of the corresponding Bessel coefficients f_n^1, the shape of spectrum lines is determined by the function $S(v_n,\beta,\eta)$ (Fig. 3). The induced angle θ_H is involved in the argument β; emission into the angle θ off the axis is taken into account in the argument η; the maximum of the function is equal to unity: $\max S = 1$.

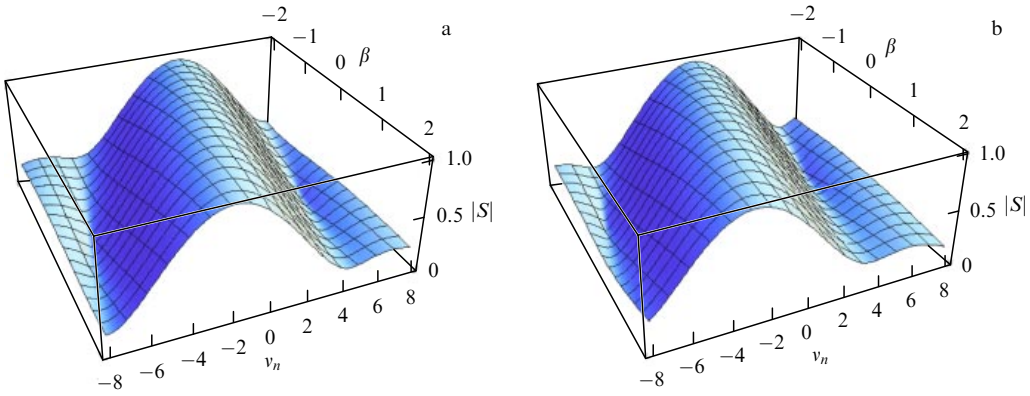

Figure 3. (Color online.) Absolute values of the function $S(\alpha, \beta)$ depending on detuning parameter v_n and argument β for (a) $\eta = 0$ and (b) $\eta = 1$.

The angles θ_H and θ can partially compensate the effect of one another. For the spectral line maximum to be preserved at the point $v_n = 0$, i.e., without detuning the spectrum frequencies, the condition

$$v_n \approx -(\beta + \eta) \quad \text{for} \quad v_n, \beta, \eta \in [-2\pi, 2\pi] \tag{38}$$

must be satisfied (see Fig. 3). It follows from (38) that the compensation resulting in $v_n = 0$ is only possible at the angle

$$\theta = \frac{2\pi}{3}\,\frac{k}{\gamma}\,N\,\frac{\kappa^2 + \rho^2}{\rho\sin\varphi - \kappa\cos\varphi}\,.$$

With no loss of generality, we assume for simplicity that only one component of the permanent field is present, $\rho = 0$; in the direction $\varphi = \pi$, we then conclude that emission into the angle $\tilde{\theta}$ occurs at the unchanged UR resonance frequency $v_n = 0$:

$$\tilde{\theta} = \frac{2\pi}{3}\,\frac{k}{\gamma}\,N\kappa = \sqrt{3}\theta_H\,.$$

The UR resonance frequencies involve the angles θ_H induced by the permanent field:

$$\omega_n = \frac{2n\omega_0\gamma^2}{\left(1 + \dfrac{k^2}{2}\right) + (\gamma\theta)^2 + (\gamma\theta_H)^2 - \gamma^2\sqrt{3}\theta_H\theta\,\dfrac{\rho\sin\varphi - \kappa\cos\varphi}{\sqrt{\kappa^2 + \rho^2}}}\,. \tag{39}$$

Hence, the permanent component κH_0 leads to a bend of the electron trajectory at the angle θ_H, and the radiation propagating along the undulator axis at the angle $\theta = -\theta_H$ to the direction of motion of the electron has resonances at the frequencies

$$\omega_n \cong \frac{2n\omega_0\gamma^2}{1 + k^2/2 + 0.27(\gamma\theta_H)^2}\,.$$

For even harmonics, due to the θ_H angle, the UR spectral line shape is determined by the function $\partial S/\partial v_n$, as shown in Fig. 4; its maximum is equal to 0.5: $\max \partial S/\partial v_n = 0.5$.

We note that the factor

$$\frac{2}{k}\,\gamma\theta_H\sqrt{3}\,\frac{\partial S}{\partial v_n}\,J_n^n$$

appearing in (28) has the same structure as regards the angle $\gamma\theta_H$ as does the angular part $\sim\gamma\theta$ in $f^2_{n;x,y}$ (see (13), (15), (17), etc.). Moreover, given the coefficient $\sqrt{3}$ present in that factor in (28) and in view of the behavior of $\partial S/\partial v_n$, we obtain

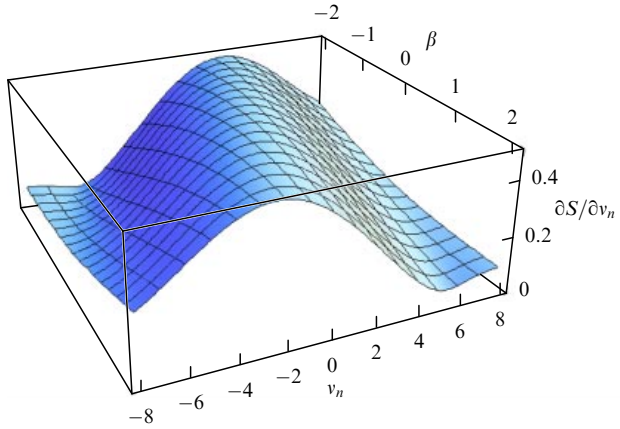

Figure 4. (Color online.) Absolute values of the function $\partial S/\partial v_n$ depending on the detuning parameter v_n and the argument β at $\eta = 0$.

$$f_n^{\,3} = \frac{2}{k}\,\gamma\theta_H\sqrt{3}\,\max\frac{\partial S}{\partial v_n}\,J_n^n \cong \frac{1.73}{k}\,\gamma\theta_H J_n^n\,, \tag{40}$$

which is similar to the expression present in the angular part of $f^2_{n;x,y}$: $(2/k)\gamma\theta J_n^n$. Thus, to estimate the contribution of the angle θ_H, we can use the standard expressions for $f^2_{n;x,y}$ from (5)–(7), (13), (15), (17), etc. with $\theta \to \theta_H$. We also note that the angle θ_H is induced by the field

$$H\,[\mathrm{T}] = \frac{\sqrt{3}\,\gamma\theta_H}{2\pi\lambda_{\mathrm{u}}\,[\mathrm{cm}]\,N}\,,$$

and a rather weak magnetic field is required in order to create a significant angle $\gamma\theta_H \approx 0.1$. For example, in the LCLS FEL undulator with $L = 3.4$ m, the field $H = 0.8$ G only slightly exceeding Earth's field is required for the angle $\gamma\theta_H = 0.1$. Naturally, such fields are carefully compensated and screened. Nevertheless, as we show in Section 3.2, even a beam deviation by 15–20 μm off the axis along the FEL gain length can result in considerable emission of the second harmonic in the FEL, as has been detected experimentally [34–36].

3.2 Effect of betatron oscillations

The contribution of betatron oscillations to UR has been studied well (see, e.g., [39–45, 57]). We recall that the simplest

harmonic dependence of the field on the coordinate along the undulator axis, $H_y = H_0 \sin(k_\lambda z)$, does not satisfy the Maxwell equations; additional components, for example, $H_y = H_0 \sin(k_\lambda z)\cosh(k_\lambda y)$ and $H_z = H_0 \cos(k_\lambda z)\sinh(k_\lambda y)$, are considered for the Maxwell equations to be satisfied in the entire gap of the undulator. This leads to the appearance of betatron oscillations at the frequency

$$\omega_\beta = \frac{\sqrt{2}\pi ck\delta}{\lambda_n n\gamma} \cong \frac{2\sqrt{2}\pi c\gamma k\delta}{\lambda_u\{1+(k^2/2)[1+(d/p)^2+(d_1/h)^2+(d_2/l)^2]\}}, \quad (41)$$

where, for the standard planar undulator, $\delta = 1$ and $d = 0$; the frequency $\omega_\beta \propto \omega_n/\gamma$ is much lower than the UR resonances ω_n for $\gamma \gg 1$. In modern FELs, ultrarelativistic electrons with $\gamma \approx 10^3 - 10^4$ are used and UR line splitting is barely visible. We note that a detailed analysis of UR with betatron oscillations taken into account was recently done in [23] for a two-frequency undulator with field (16). In the case of multiperiodic fields in an undulator, the physics of betatron oscillations is essentially the same. We obtain Bessel coefficients (5), (6), (13), (15), (17), (19), and (20) (depending on the undulator field harmonics) factored through the following generalized Bessel functions, which occur due to betatron oscillations:

$$f_n^{1,2} \to \sum_p \tilde{J}_p(\xi,\zeta) f_n^{1,2}, \qquad \tilde{J}_p(\xi,\zeta) = \frac{1}{2\pi}\int_0^{2\pi} \cos\left[pq - \zeta\sin q - \xi\sin(2q)\right] dq, \quad (42)$$

with the arguments involving the off-axis deviation of the electron by y_0:

$$\xi = \frac{\pi^2 y_0^2 k\delta}{2n\gamma\sqrt{2}\,\lambda_u\lambda_n} \approx \frac{\pi^2\gamma y_0^2 k\delta}{\sqrt{2}\lambda_u^2(1+k^2/2)}, \qquad \zeta = \frac{2\pi\theta y_0}{n\lambda_n} \approx \frac{4\pi\theta y_0\gamma^2}{\lambda_u(1+k^2/2)}. \quad (43)$$

In FELs where beams of relativistic electrons are used, the coefficient $\tilde{J}_{p=0}$ is in many cases close to unity, and the other coefficients $J_{p=\pm1,2,3\ldots}$ are small, $\sim 10^{-1} - 10^{-2}$. But even if the splitting of spectrum lines is considerable, the p subharmonics are positioned close to each other, at the distance $\delta\lambda = \lambda k/\sqrt{2}\gamma$; for relativistic beams, $\delta\lambda/\lambda$ is typically much less than the relative width of the UR spectrum lines and the Pierce parameter ρ, which gives an estimated value of the spectral density of FEL emission. We note that the splitting of UR spectrum lines can be due to a combination of the off-axis deviation by y_0 and emission at an angle θ entering argument ζ. Numerical estimates are given in Section 4, where we study the origin of the strong second harmonic in the X-ray FEL LCLS [35, 36] and in the LEUTL (Low-Energy Undulator Test Line) FEL [37, 38] emitting in the optical and long-wavelength ultraviolet (UV-A) ranges.

Even harmonics of a planar undulator occurring due to betatron oscillations are well known; they have the following Bessel coefficients, to which the more complicated expression for a two-frequency undulator in [23] also reduces:

$$f_{n,p;y}^4 \cong \frac{\sqrt{2}\pi y_0\delta}{\lambda_u}\left(\tilde{J}_{p+1}(\xi,\zeta) - \tilde{J}_{p-1}(\xi,\zeta)\right)\tilde{J}_n(\bar{\xi},\bar{\zeta}), \quad (44)$$

where

$$\bar{\xi} = -\frac{1}{8}\frac{k^2}{\gamma^2}\frac{\lambda_u}{\lambda_n} = -\frac{1}{4}\frac{nk^2}{1+k^2/2}, \quad \bar{\zeta} = \frac{8\bar{\xi}\gamma\theta}{k},$$

with ξ and ζ defined in (43). For the planar undulator field with harmonic (16), $H_y = H_0[\sin(k_\lambda z) + d\sin(pk_\lambda z)]$, calculations performed in [23] give Bessel coefficient (17) with factor (42), as was to be expected. The undulator field harmonic d makes a contribution to $\delta = \sqrt{1+d^2}$ and to the resonance of radiation wavelengths

$$\lambda_n = \frac{\lambda_u}{2n\gamma^2}\left[1 + \frac{k^2}{2}\left(1 + \left(\frac{d}{p}\right)^2\right)\right].$$

Instead of $\tilde{J}_n(\bar{\xi},\bar{\zeta})$ for the two-frequency undulator, expression (44) involves J_n^n (see the angular part of $f_{n;y}^2$ in (17) and in [23] in another notation); the functions J_n^n are the limiting case of (7) for $d_1 = d_2 = h = l = 0$. The contribution of betatron oscillations is generalized to the case of multiperiodic undulator field (2) with nonzero $d_{1,2}$, p, h, and l in (7)–(11) and $\delta = (1 + d^2 + d_1^2 + d_2^2)^{1/2}$ in ω_β: in expression (44), we use $J_n^n(\xi_i)$ in (7) instead of $\tilde{J}_n(\bar{\xi},\bar{\zeta})$.

Thus, the nth UR harmonic is split into p subharmonics. This splitting is insignificant because $\omega_\beta \propto \omega_n/\gamma$. As a result, for $p = 0$ we have $f_{n,p=0;y}^4 \sim 10^{-2}$; for other p we obtain even lower values, and the contribution to the generation of even harmonics due to betatron oscillations and the corresponding Bessel coefficients $f_{n,p;y}^4$ are small compared with (5), (6), (13), (15), and (17), where $f_{n=1,3,5}^{1,2} \sim 0.15 - 0.8$. Examples pertaining to real FEL installations are given in Section 4, where we discuss some FEL experiments using an analytic model (see the Appendix) involving the logistic function [58–60].

4. Modeling the generation of harmonics in experiments with free-electron lasers

Deviations of an electron beam from the undulator axis are typically small; however, even a deviation by $\sim 5-25$ μm over the gain length of an X-ray FEL can change the spectral content of emission. In experiments with the X-ray LCLS FEL, the centering of the electron beam on the axis was required to be 5 μm over the gain length $L_g = 1.6-3.5$ m, whereas the available methods for control and adjustment had an accuracy of 50 μm [34–36]. The deviation of a beam electron with energy $E = 13.6$ GeV by just 10 μm over the gain length $L_g \approx 3$ m leads to a considerable effective bend angle $\theta\gamma \approx 0.1$. This can affect the emission, as we show in what follows. In the LEUTL FEL, the beam has an order of magnitude greater size, ~ 0.2 mm. To model and analyze the effect of various factors on the power of harmonics emitted by an FEL, we use the analytic FEL model [52], which has been tuned in FEL experiments, together with a description of the oscillation power in the saturation mode (see the Appendix), and the analytic expressions for Bessel coefficients derived in Sections 2 and 3 with the angles and corrections for betatron oscillations in a finite-size beam taken into account.

In LCLS experiments [35, 36], X-ray radiation was generated in the range of $1.5-20$ Å. The installation consists of 33 undulator sections, each 3.4 m in length. Undulators with permanent magnets have the period $\lambda_u = 3$ cm, parameter $k = H_0\lambda_u e/(2\pi mc^2) = 3.5$, and the electron current is 1–3.5 kA. In experiments with X-ray radiation whose main pitch wavelength is $\lambda_1 = 1.5$ nm, the second and third

Table. Some data on the modeling* of the LCLS experiment with $\lambda = 1.5$ nm.

FEL harmonic number	$n = 1$	$n = 2$	$n = 3$	$n = 5$
Bessel coefficient accounting for off-axis beam drift by 15 μm over a length of 1.5 m Bessel coefficient f_n for on-axis beam	0.742 0.744	**0.075** *0.025*	**0.330** *0.338*	**0.213** *0.229*
Pierce parameter $\tilde{\rho}_n$ accounting for off-axis beam drift by 15 μm over a length of 1.5 m Pierce parameter $\tilde{\rho}_n$ for on-axis beam	0.0010 0.0010	**0.0002** *0.0001*	0.0006 0.0006	0.0005 0.0005
Harmonic wavelength λ_n, nm	1.5	0.75	0.5	0.3
Saturation power accounting for off-axis beam drift by 15 μm over a length of 1.5 m, $P_{F,n}$, W Saturation power for on-axis beam, $P_{F,n}$, W	5.5×10^9 7×10^9	$\mathbf{1.5 \times 10^6}$ 10^4	$\mathbf{1.2 \times 10^8}$ 2×10^8	$\mathbf{1.3 \times 10^7}$ 2×10^7

* Electron beam parameters: energy $E = 4.3$ GeV, $\gamma = 8400$, beam power $P_E = 4.29$ TW, current $I_0 = 1$ kA, current density $J = 2.23 \times 10^{11}$ A m^{-2}, cross section $\Sigma = 2\pi\sigma_x\sigma_y = 4.79 \times 10^{-9}$ m^2, emittance at injector $\gamma\varepsilon_{x,y}^{135\ \mathrm{meV}} = 0.4$ μm, emittance at projection on undulators $\gamma\varepsilon_{x,y}^{4.3\ \mathrm{GeV}} \approx 0.6$ μm, Twiss parameter $\beta = 10$ m, transverse size $\sigma_{x,y} \approx 27$ μm, divergence $\theta_{\mathrm{div}} \approx 2.7$ mrad, and energy spread $\sigma_e = 0.3 \times 10^{-3}$. Undulator parameters: $k = 3.5$, $\lambda_u = 3$ cm, $N = 113$, and section length = 3.4 m. Calculated FEL parameters: saturation length $L_s \approx 25$ m, gain length $L_{\mathrm{gain}} \approx 1.5$ m, and photon beam size $\sigma_{\mathrm{photon}} \cong 19$ μm.

harmonics were detected. According to [36], in most cases the measured power of the third harmonic was $\approx 2-2.5\%$ of the main pitch power, the measured power of the second harmonic was $\sim 0.04-0.1\%$ of the main pitch in the normal mode of the FEL [36], while the fifth harmonic was not measured, but numerical simulations suggest that its power is $\sim 10\%$ that of the third harmonic. It was noted in [35, 36] that in some cases the magnitude of higher FEL harmonics decreased by an order of magnitude and additional studies were needed, especially as regards the strong second harmonic. We modeled this experiment. The main results are collected in the table.

The evolution of the power of FEL harmonics along the undulator length is illustrated in Fig. 5; the measured power of the harmonics is shown with colored bands in the saturation domain on the right-hand side of Fig. 5, taking the spread of the measured power of the harmonics into account (see [36]). The saturation and gain lengths and the main pitch power of the FEL exactly reproduce the experimental data in [34–36]. Higher FEL harmonics also fit the measurement error well (see Fig. 5). We note that the field harmonics themselves cannot cause the appearance of a strong second UR harmonic; they mainly affect the intensity of the third and fifth harmonics [50, 52] as well as the saturation length and power of these harmonics in an FEL. The leading correction to the radiation spectrum is due to the third harmonic of the undulator magnetic field [49], the other field harmonics producing little effect. Even a perceptible presence of field harmonics of $\sim 10\%$ of the main undulator field strength hardly changes the emission characteristics of FELs such as LCLS [52].

We investigated the behavior of FEL harmonics as a function of the beam parameters analytically. Using a phenomenological FEL model, we took the dependence of Bessel coefficients on the angles and the beam size into account, together with all the corrections due to the energy spread, emittance, diffraction, etc. The respective values of the FEL parameters for a beam centered on the axis and with its off-axis deviation by 15 μm over the gain length $L_{\mathrm{gain}} \approx 1.5$ m are shown in the Table with *italic* and **boldface** fonts for visual clarity. The analysis confirms the conclusion in [36] that "the proportion of the third harmonic decreases as the FEL performance and beam quality degrade."

In the case of beam centering to within 5 μm of the undulator axis, we obtained a theoretical value of the third harmonic power somewhat exceeding the one in Fig. 5

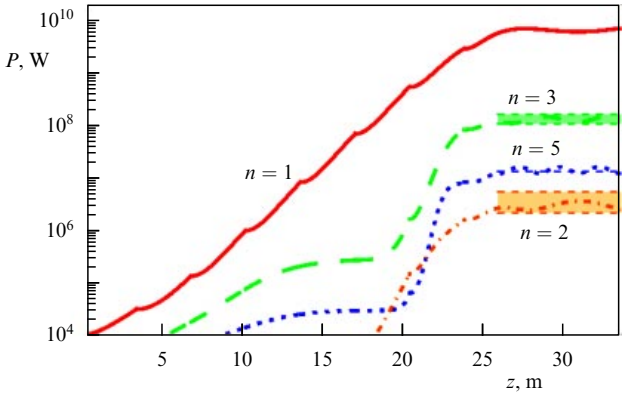

Figure 5. (Color online.) Evolution of the power of FEL harmonics in the LCLS experiment with $E = 4.3$ GeV, $\lambda_1 = 1.5$ nm, $\sigma_e = 0.3 \times 10^{-4}$, and $I_0 = 1$ kA. The $n = 1$ harmonic corresponds to the red solid line, the $n = 2$ harmonic to the dashed-dotted orange line, $n = 3$ to the green dotted line, and $n = 5$ to the blue dotted line. Colored strips on the right show the experimentally admissible ranges of the measured quantities. The fifth harmonic power estimate is $P_5 \approx 0.1P_3$.

(somewhat above the upper boundary of the green domain on the right in Fig. 5). At the ideal centering, the theoretical power of the second harmonic was significantly lower than the one measured in experiment. We carefully estimated the contribution of betatron oscillations: the corresponding Bessel coefficients turned out to be negligibly small: $f_{n,p;y}^4 \sim 2 \times 10^{-3}$. This can be compared with the second-harmonic Bessel coefficients due to emittance alone, which are an order of magnetic higher: $f_{2;y} \sim 0.025$. In the LCLS experiment with electron energy $E_e = 4.3$ GeV [36], an off-axis drift of beam trajectories by 10–20 μm over the gain length $L_{\mathrm{gain}} \approx 1.5$ m was observed (see [34, 35]). This off-axis deviation of the beam is comparable to the photon beam size $\sigma_{\mathrm{photon}} \equiv \sigma_\gamma \approx [\sigma_{x,y}\sqrt{\lambda_1 L_g/(4\pi)}\,]^{1/2} \approx 20$ μm.

We note that the target deviation of the beam in the installation was 5 μm, and adjustment methods allowed reliably controlling the deviation of 50 μm. With a 5-μm minimal deviation, we obtain a theoretical value of the FEL second harmonic power of ~ 10 kW and the minimal UR line splitting $\tilde{J}_{p=-1,0,1}(\xi, \zeta) = \{0.1, 0.98, 0.1\}$. Given the size of the photon beam and the actual centering of the electron beam attainable to within ~ 15 μm, we obtain an FEL second harmonic power within the range of measured values (see the dashed-dotted orange line and the orange domain in Fig. 5).

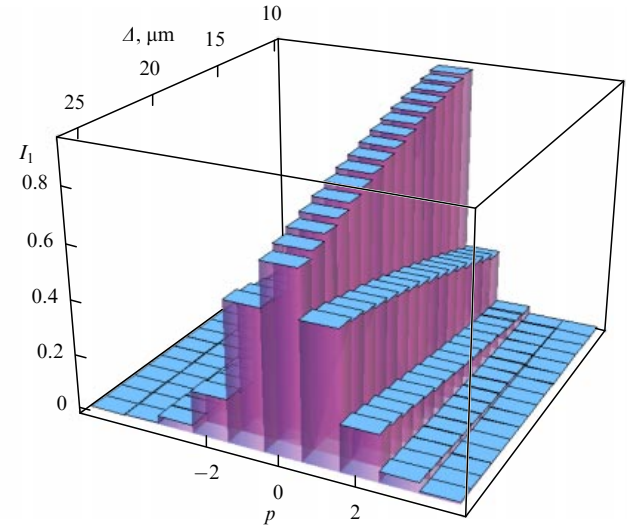

Figure 6. Splitting of the main pitch spectrum line $\lambda = 1.5$ nm at the p subharmonic as a function of the distance Δ from the axis in the LCLS FEL.

Other harmonics also fall in the range of measured quantities. The corresponding effective angle is then given by $\theta \approx 9$ mrad, $\theta\gamma \approx 0.08$, but UR line splitting due to betatron oscillations remains small, as is evidenced by the Bessel function values for the p subharmonics: $\tilde{J}_{p=-2,1,0,1,2}(\xi,\zeta) = \{0.06, 0.34, 0.87, 0.34, 0.07\}$.

The contribution of subharmonics and the main pitch spectrum line splitting $\lambda_1 = 1.5$ nm depending on the distance from the axis are shown in Fig. 6.

As a result of the high energy of electrons in the beam, $E \approx 4.3$ GeV, the UR spectrum line splits by a very small quantity $\delta\lambda = \lambda_1 k/(\gamma\sqrt{2}) \approx 0.0005$ nm, and the deviation of subharmonics of wavelength $\lambda_1 = 1.5$ nm and its resonances λ_1/n is negligibly small. Given the splitting (see Fig. 6), we have a theoretical linewidth $\Delta \sim 2$ pm and relative spectral density $\Delta/\lambda_1 \sim 0.15\%$. The emitted subharmonics $p = 0, \pm 1, \pm 2$ are within the natural width of the spectrum line, and the electrons in the beam interact with all the subharmonics of the nth FEL harmonic, even at significant off-axis deviations of the beam, as was registered in the LCLS experiment. We note that the equivalent angle $\gamma\theta_H = 0.08$ can be caused by field strength $H \approx 1.4$ G, which is ~ 2.5 times stronger than Earth's field; such a field must always be compensated.

In the LEUTL experiment [37], radiation in the UV-A and optical ranges was generated at the wavelengths $\lambda_1 = 385$ and 532 nm; the size of the electron and photon beams was an order of magnitude greater than in the LCLS FEL: $\sigma_{x,y} \approx 0.26$ mm, $\sigma_\gamma \approx 0.2$ mm; the angle of divergence $\theta \sim 0.15$ mrad was almost two orders of magnitude greater than in the LCLS FEL. Under such conditions, betatron oscillations can be assumed to exert a significant effect on LEUTL FEL emission. Calculation of the Bessel coefficients $f^{1,2}$ in (17) for x- and y-polarizations with the beam divergence $\gamma\theta_{\rm div} \approx 0.07$ gives the values

$$f^{1,2}_{n=1,\ldots,5;\,x} \approx \{0.75, 0.07, 0.34, 0.07, 0.23\}\,,$$

$$f^{1,2}_{n=1,\ldots,5;\,y} \approx \{0, 0.015, 0, 0.015, 0\}\,.$$

The spectrum splitting caused by betatron oscillations is small because $\gamma \approx 500 \gg 1$. Furthermore, at $\gamma\theta_{\rm div} = 0.07$, the splitting is expressed weakly: the fundamental subharmonic with $p = 0$ and $\tilde{J}_{p=0} \approx 1$ is mainly present. For the second FEL emission harmonic, $n = 2$, we obtain the following Bessel coefficients (44) for the $p = \{0, \pm 1, \pm 2, \pm 3\}$ subharmonics due to betatron oscillations:

$$f^{4}_{n=2,\,p=0,\,\pm1,\,\pm2,\,\pm3} \cong \{0.012,\, 0.008,\, 0.005,\, 0.002\}\,,$$

whose total contribution is small: $\sqrt{\sum_p (f^4_{n=2,\,p})^2} \sim 0.014$. This is comparable to the contribution made by the divergence angle $\theta_{\rm div}$ for the y-polarization of UR, $f_{n=2,\,y} \approx 0.015$, but is less than the contribution of the divergence angle $\theta_{\rm div}$ for the main, x, polarization: $f_{n=2,\,x} \approx 0.04$. But even with all these factors taken into account, the calculated power of the second harmonic is much less than the one measured in experiment.

To explain the high power of the second harmonic in the LEUTL experiment, we recall that the angle of interaction of radiation with electrons in a wide beam $\sigma_{x,\,y} \sim 0.2$ mm in size over the gain length $L_{\rm gain} \approx 0.88$ m is $\bar{\theta} \approx \sigma_{x,\,y}/L_{\rm gain} \approx 2.4 \times 10^{-4}$ rad, or $\gamma\bar{\theta} \approx 0.12$, which is greater than the divergence angle $\theta \approx 1.4 \times 10^{-4}$ rad. Because of the effective angle of electron–photon interaction $\bar{\theta}$, subharmonics with $p = \{0, \pm 1\}$ appear, $\tilde{J}_{p=-1,0,1} = \{0.22, 0.95, 0.19\}$, but the UR lines split by the small quantity $\delta\lambda/\lambda \sim 1/\gamma \ll 1$ because $\gamma \approx 500 \gg 1$. The Bessel coefficients are then as follows:

$$f_{n=1,\ldots,5;\,x} \approx \{0.75, 0.14, 0.31, 0.15, 0.18\}\,,$$

$$f_{n=1,\ldots,5;\,y} \approx \{0.006, 0.04, 0.010, 0.026, 0.012\}\,.$$

For the even harmonics, the Bessel coefficients are several times greater, and for the odd, somewhat less than in the case where only the beam divergence is taken into account (see above). The contribution of betatron oscillations (44) to the emission of even harmonics remains small, comparable to the angular contribution of y-polarized emission (17): $f^{\beta}_{n=2,\,p} \approx 0.03 \sim f_{n=2,\,y} \approx 0.04$. For emission with x-polarization, which constitutes the main part of the emission, we have a much greater Bessel coefficient for the second harmonic, $f_{n=2,\,x} \approx 0.14$, which exceeds the corresponding coefficient for y-polarized emission $f_{n=2,\,y}$ and the betatron contribution $f^{\beta}_{n=2,\,p}$ (see above). Taking all this into account, we obtain the emission power for all the LEUTL FEL harmonics in agreement with the experimental values in [37, 38], as is shown in Figs 7 and 8.

We note that the analytic description of LEUTL experiments is more precise than the numerical simulation by the authors of the experiment in [36, 37].

To conclude, we give the results of analytic modeling of the high-current SACLA experiment (Spring-8 Angstrom Compact free-electron LAser) [61] with electron energy $E = 7.8$ GeV, electron bunch duration $\tau_{\rm e} = 10$ fs, current $I = 27$ kA, energy spread $\sigma_{\rm e} = 0.087\%$, emittance $\gamma\varepsilon = 0.6$ μm, and emission at the wavelength $\lambda_1 \approx 0.125$ nm from undulators with $k = 2.115$ and period $\lambda_{\rm u} = 1.8$ cm. We thus obtain photon pulse duration $\tau_\gamma \sim 6.3$ fs, a gain length of ≈ 2.1 m, and saturation after 32 m with a power of ~ 70 GW, in accordance with [61]. Experimental values are shown with dots; the power values obtained in the model are shown with colored curves in Fig. 9a. The fractions of the power of the harmonics in the saturation mode are $\sim 0.4\%$ for $n = 3$, $\sim 0.01\%$ for $n = 5$, and 0.006% for $n = 2$.

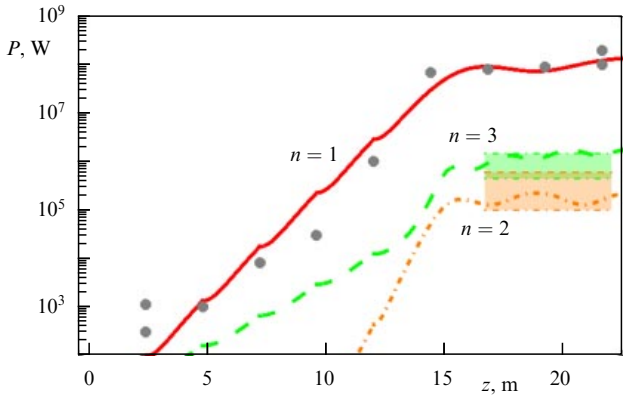

Figure 7. (Color online.) Evolution of the power of FEL harmonics in the LEUTL experiment with $E = 255$ MeV, $\lambda_1 = 385$ nm, $\sigma_e = 1 \times 10^{-3}$, and $I_0 = 184$ A. The $n = 1$ harmonic is shown with the red solid line, $n = 2$ with the orange dashed-dotted line, and $n = 3$ with the green dotted line. Colored areas on the right-hand side of the figure show the harmonic power ranges evaluated by the authors of the experiment. Experimental values are shown by dots.

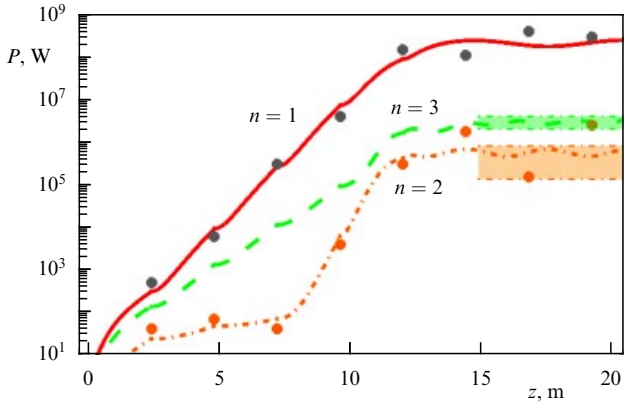

Figure 8. (Color online.) Evolution of the power of FEL harmonics in the LEUTL experiment with $E = 217$ MeV, $\lambda_1 = 532$ nm, $\sigma_e = 1 \times 10^{-3}$, and $I_0 = 210$ A. The $n = 1$ harmonic is shown with the red solid line, $n = 2$ with the orange dashed-dotted line, and $n = 3$ with the green dotted line. Colored areas and dashed-dotted lines on the right-hand side of the figure show the harmonic power ranges evaluated by the authors of the experiment. Experimental values are shown by dots.

Using the theory expounded in Section 3 together with the generalized special Bessel and Airy functions, we theoretically calculated the shape and width of the emission spectral line (Fig. 9b). The spectral density of emission at the wavelength of the main pitch is determined by splitting into more than 20 subharmonics and amounts to $\approx 0.2\%$. This agrees well with the experimental result for the spectral width of ≈ 30 eV for photons with an energy of 9.85 keV and the corresponding density of $\approx 0.3\%$ (see Fig. 2 in [61]).

The most recent results of other experiments with X-ray FELs also confirm the validity of our theoretical approach to the investigation of characteristics of FEL emission [62–64].

A comparison of the above analytic results and FEL experiments shows that the results of our theoretical analysis are virtually no worse in accuracy than those of numerical modeling on powerful computers, done by large groups of developers and researchers with the use of sophisticated three-dimensional numerical simulations within appropriate computational platforms. The above analytic formalism is applicable to virtually any FEL undulator; it allows investigating the generation of harmonics in FEL undulators using a personal computer with standard software, explains the origin of harmonic generation, and corresponds well with experiments.

5. Conclusions

We have theoretically investigated the generation of UR harmonics in undulators with field harmonics and with the off-axis effect and nonperiodic magnetic components taken into account. We obtained exact analytic expressions for the Bessel coefficients and the intensity and spectrum of the emission of relativistic electrons in quadratures expressed through elementary functions. For a generalized elliptical undulator with two different field harmonics in both polarizations, we obtained exact analytic results in the form of generalized Bessel and Airy functions. The effect that the finite size of the electron beam, the divergence, and the electron energy spread exert on the characteristics of emission were taken into account. We studied the possible effect of permanent magnetic field components on the spectrum and the intensity and shape of UR lines. The results are obtained in integral form for an arbitrary undulator.

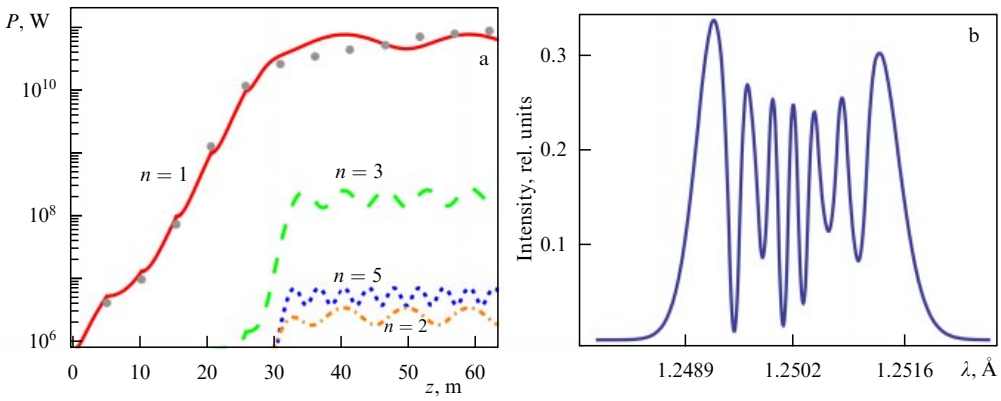

Figure 9. (Color online.) (a) Evolution of the power of FEL harmonics in the high-current SACLA experiment with $E = 7.8$ GeV, $\sigma_e = 0.87 \times 10^{-3}$, $I_0 = 27$ kA, and $\lambda_u = 1.8$ cm. The $n = 1$ harmonic ($\lambda_1 = 0.125$ nm) is shown with the red solid line, $n = 2$ with the orange dashed-dotted line, $n = 3$ with the green dotted line, and $n = 5$ with the blue dotted line; experimental values are shown by dots. (b) Theoretically calculated spectrum line of the main pitch.

The obtained exact analytic expressions for Bessel coefficients of the UR harmonics take all the main losses in real installations into account. They are used in an analytic FEL model to study the evolution of the power of the harmonics of a single-pass FEL along the undulator length. We investigated the generation of FEL harmonics in the LCLS experiment in the X-ray range and in the LEUTL experiment in the optical and longwavelength ultraviolet ranges. The second harmonic registered in experiments cannot be caused by the undulator field harmonics, which can affect only the odd UR harmonics. The analytic form of all the obtained expressions has allowed us to study the contributions of each component of the Bessel coefficients separately. We have shown that the electron beam emittance in the X-ray LCLS FEL alone cannot cause a second harmonic with the intensity registered in experiment. The contribution of betatron oscillations to the generation of even harmonics also turns out to be negligibly small; also small is the UR line splitting induced by betatron oscillations in the LCLS experiment. The second harmonic generation for soft X-ray LCLS FEL emission is explained by the observed deviation of the electron beam trajectory from the axis by ~ 15 μm over the FEL length of ~ 1.5 m; such a deviation is comparable to the photon beam size. This gives rise to substantial angular contributions, taken into account analytically, which lead to the considerable power of the second harmonic in the FEL. The results of our modeling of the evolution of FEL harmonics in LCLS undulators with the use of analytic expressions exactly agrees with experimental data (see Fig. 5). The spectral width of emission at the main pitch wavelength $\lambda_1 = 1.5$ nm with the theoretically calculated splitting (see Fig. 6) amounts to $\sim 0.15\%$, which is comparable to the Pierce parameter value $\rho \approx 10^{-3}$. In the LEUTL experiments in the optical range and in the UV-A range, including only the betatron effects and the emittance of a wide electron beam gives a theoretic power of the second harmonic of the emission that is two orders of magnitude less than in the experiment. The measured values of the second harmonic power in the LEUTL experiments are explained by the significant angle $\gamma\bar{\theta} \approx 0.1$ of the electron–photon interaction in a wide beam ~ 0.2 mm in size over the gain length $L_{\text{gain}} \approx 0.88$ m. Taking this into account, we obtain several-fold greater Bessel coefficients for even harmonics and somewhat lower values for odd harmonics; theoretical results for the evolution of the power of FEL harmonics agree with experimental data (see Figs 7 and 8).

Thus, the detailed analysis of the generation of harmonics in FELs with the use of the obtained exact analytic expressions for the Bessel coefficients and analytic formulas for the dynamics of the FEL power has allowed selecting and analyzing the contributions of all the main factors to the generation of each FEL harmonic. Our theory explains the physical reasons behind the generation of emission harmonics in different conditions. In particular, the measured second harmonic in the X-ray LCLS FEL is explained by the experimentally observed deviation of the electron beam from the axis by ≈ 15 μm, comparable to the photon beam size; the powerful second harmonic in the LEUTL FEL occurs due to wide, ~ 200 μm, electron and photon beams and the corresponding large angle of the electron–photon interaction.

The modeling of the recent SACLA FEL experiment also confirms the validity of our theoretical approach. The calculated evolution of the emission power, saturation, spectral line shape, and spectral density are fully consistent with the experimental data.

Our analytic description of spectrum lines and the intensity of spontaneous and induced UR allows us to select and analyze all the contributions to harmonic generation in the emission. The use of the obtained results make it possible to analytically investigate the effect of different characteristics of the beam and of the magnetic field on the generation of FEL harmonics. This can also be used to assess the quality of the beam and its centering in undulators based on the emission characteristics.

6. Appendix. Phenomenological model of a single-pass free-electron laser

An effective description of the evolution of the power of harmonics along the FEL length with diffraction taken into account involves the Pierce parameter ρ_n [12, 13, 60]:

$$\tilde{\rho}_n = \frac{\rho_n}{(1+\mu_{D,n})^{1/3}}\,, \qquad \rho_n = \frac{J^{1/3}(\lambda_{\text{u}} k_{\text{eff}} f_n)^{2/3}}{2\gamma(4\pi i)^{1/3}}\,, \qquad \mu_{D,n} = \frac{\lambda_{\text{u}}\lambda_n}{16\pi\rho_n \Sigma}\,, \tag{45}$$

where n is the number of the harmonic, $\Sigma = 2\pi\sqrt{\beta_x\varepsilon_x\beta_y\varepsilon_y}$ is the cross section of the beam, $\varepsilon_{x,y} = \sigma_{x,y}\theta_{x,y}$ is its emittance, $\sigma_{x,y} = \sqrt{\varepsilon_{x,y}\beta_{x,y}}$ is the transverse cross section, $\theta_{x,y}$ is the divergence, $\gamma_{x,y}$ and $\beta_{x,y} = \varepsilon_{x,y}/\theta_{x,y}^2$ are the Twiss parameters, $J = I_0/\Sigma$ [A m^{-2}] is the current density, I_0 [A] is the electron current, $i \approx 1.7045 \times 10^4$ A is the Alfvén constant, λ_{u} [m] is the fundamental period of the undulator, λ_n is emission wavelength (4), k_{eff} is the undulator parameter (for a planar undulator, $k_{\text{eff}} = k = eH_0\lambda_{\text{u}}/(2\pi mc^2) \approx H_0\lambda_{\text{u}}$ [T cm]), H_0 is the magnetic field amplitude on the undulator axis, and f_n are the Bessel coefficients of the nth harmonic (see (5) and (6)). The Pierce parameter $\tilde{\rho}$ determines the gain length $L_{n,\text{g}} \cong \Phi_n\lambda_{\text{u}}/(4\pi\sqrt{3}\,n^{1/3}\tilde{\rho}_n)$ for the nth harmonic: $L_{1,\text{g}} \equiv L_{\text{g}}$. The corrections describing the loss in an FEL are taken into account phenomenologically as

$$\Phi_n \cong (\zeta^n + 0.165\mu_{\varepsilon,n}^2)\exp(0.034\mu_{\varepsilon,n}^2)\,, \quad \tilde{\Phi}_n = \Phi_n\big|_{\mu_{\varepsilon,n}\to\tilde{\mu}_{\varepsilon,n}}\,, \tag{46}$$

$$\mu_{\varepsilon,n}(\sigma_\varepsilon, n) \cong \frac{2\sigma_\varepsilon}{n^{1/3}\rho_n}\,, \quad \tilde{\mu}_{\varepsilon,n}(\sigma_\varepsilon, n) \cong \frac{2n^{2/3}\sigma_\varepsilon}{\tilde{\rho}_n}\,, \tag{47}$$

$$\eta_n \cong \frac{\exp\left[-\Phi_n(\Phi_n - 0.9)\right] + 1.57(\Phi_n - 0.9)/\Phi_n^3}{1.062}\,, \qquad \tilde{\eta} = \eta_n\big|_{\Phi_n\to\tilde{\Phi}_n}\,, \tag{48}$$

$$\zeta \cong \sqrt{\prod_{i=x,y,\tilde{x},\tilde{y}}(1+\mu_i^2)} \times \left(1 + 0.159\sum_{i=x,y,\tilde{x},\tilde{y}}\mu_i^2 - 0.066\sum_{i=x,y,\tilde{x},\tilde{y}}\mu_i\right)^{-1}, \tag{49}$$

$$\mu_{\tilde{x},\tilde{y}} = \frac{1}{\tilde{\rho}_1}\frac{\gamma^2\varepsilon_{x,y}}{(1+k_{\text{eff}}^2)\lambda_{\text{u}}\beta_{x,y}}\,, \quad \mu_{x,y} = \frac{1}{\tilde{\rho}_1}\frac{\gamma^2\pi^2k^2\varepsilon_{x,y}}{(1+k_{\text{eff}}^2)\gamma^2\lambda_{\text{u}}^2\gamma_{x,y}}\,. \tag{50}$$

The beam is typically adjusted to the undulator; then, $\zeta \approx 1.00-1.05$. In X-ray FELs, $\zeta \approx 1-1.02$. Phenomenological formulas (46)–(50) and formulas (51)–(53) for the power

evolution obtained by comparing them with the results of FEL experiments are substantially different from the expressions used previously in [43, 60]. They take the loss in real installations into account separately for each harmonic and allow a good description of the FEL power dynamics, including in the saturation mode. The expression describing the increase in the emission power of the nth harmonic in the z coordinate includes an independent term $\propto \exp(z/L_{n,\mathrm{g}})$ and an induced term $\propto \exp(nz/L_{\mathrm{g}})$:

$$P_n(z) \cong P_{L,n}(z) + \frac{\tilde{P}_{n,0}\exp(nz/L_{\mathrm{g}})}{1+\left[\exp(nz/L_{\mathrm{g}})-1\right]\tilde{P}_{n,0}/\tilde{P}_{n,F}} + \frac{P_{n,0}\exp(nz/L_{\mathrm{g}})}{1+\dfrac{1.3P_{n,0}\left[\exp(nz/L_{\mathrm{g}})-1\right]}{P_{n,F}\left\{1+0.3\cos\left[n(z-L_{\mathrm{s}})/(1.4L_{\mathrm{g}})\right]\right\}-0.3\tilde{P}_{n,F}}}, \quad (51)$$

where for a nonbunched electron beam we have the independent term

$$P_{L,n}(z) \cong \frac{P_{0,n}A(n,z)\exp(0.223z/L_{\mathrm{s}})}{1+\dfrac{1.3P_{n,0}\left(A(n,z)-1\right)}{P_{n,F}\left\{1+0.3\cos\left[n(z-L_{\mathrm{s}})/(1.4L_{\mathrm{g}})\right]\right\}}},$$
$$A(n,z) \cong \frac{1}{3}+\frac{\cosh(z/L_{n,\mathrm{g}})}{4.5} + \frac{\cos\left[\sqrt{3}z/(2L_{n,\mathrm{g}})\right]\cosh\left[z/(2L_{n,\mathrm{g}})\right]}{0.444}, \quad (52)$$

and for a cascade of undulators with an already bunched beam at the entrance,

$$P_{L,n}(z) \cong \frac{P_{0,n}F(n,z)}{1+1.3P_{0,n}F(n,z)/P_{n,f}\left\{1+0.3\cos\left[n(z-L_{\mathrm{s}})/(1.3L_{\mathrm{g}})\right]\right\}},$$
$$F(n,z) \cong 2\left|\cosh\left(\frac{z}{L_{n,\mathrm{g}}}\right)-\cos\left(\frac{z}{2L_{n,\mathrm{g}}}\right)\cosh\left(\frac{z}{2L_{n,\mathrm{g}}}\right)\right|, \quad (53)$$

where $L_{\mathrm{s}} \cong 1.07L_{1,\mathrm{g}}\ln(9\eta_1 P_F/P_{0,1})$ is the saturation length [60], $P_{n,F}=\eta_n P_F f_n^2/(n^{5/2}f_1^2)$ is the full saturation power and $\tilde{P}_{n,F}=\tilde{\eta}_n\tilde{P}_F f_n^2/(n^{5/2}f_1^2)$ is the preliminary saturation power, $P_F \cong \sqrt{2}P_{\mathrm{e}}\eta_1\tilde{\rho}_1^2/\rho_1$, $\tilde{P}_F = P_F|_{\eta_n\to\tilde{\eta}_n}$, $P_{0,n}$ are the initial harmonic powers, $P_{n,0} \cong nb_n^2 P_{n,F}$ and $\tilde{P}_{n,0} \cong d_n b_n^2 \tilde{P}_{n,F}$ are the initial powers induced by the main pitch due to bunching $b_n^2 \cong (P_{0,1}/9P_{\mathrm{e}}\tilde{\rho}_1)^n$, and $d_{n=1,\ldots,5} \cong \{1,3,8,40,120\}$ [60].

An additional contribution of the noise bunch emission, $P_{\mathrm{noise}} \approx 6\pi\rho^2\gamma mc^3/\lambda_1$, to the first SASE FEL cascade is described by the approximate phenomenological formula

$$N_n(z) \approx P_{\mathrm{noise}}\frac{S_n(z)}{1+\left[300P_{\mathrm{noise}}S_n(z)/(nP_{n,f})\right]},$$
$$S_n(z) \cong 2\left|\cosh\frac{z}{L_{n,g}}-\exp\left(\frac{z}{2L_{n,g}}\right)\cos\left(\frac{\pi}{3}+\frac{\sqrt{3}z}{2L_{n,g}}\right) - \exp\left(\frac{z}{2L_{n,g}}\right)\cos\left(\frac{\pi}{3}-\frac{\sqrt{3}z}{2L_{n,g}}\right)\right|, \quad (54)$$

which agrees with the experimental results (see Figs 7–9).

References

1. Ginzburg V L *Izv. Akad. Nauk SSSR Ser. Fiz.* **11** 165 (1947)
2. Motz H, Thon W, Whitehurst R N *J. Appl. Phys.* **24** 826 (1953)
3. McNeil B W J, Thompson N R *Nat. Photon.* **4** 814 (2010)
4. Pellegrini C, Marinelli A, Reiche S *Rev. Mod. Phys.* **88** 015006 (2016)
5. Schmüser P et al. *Free-Electron Lasers in the Ultraviolet and X-Ray Regime. Physical Principles, Experimental Results, Technical Realization* (Springer Tracts in Modern Physics, Vol. 258) (Cham: Springer, 2014)
6. Huang Z, Kim K-J *Phys. Rev. ST Accel. Beams* **10** 034801 (2007)
7. Margaritondo G, Ribic P R *J. Synchrotron Rad.* **18** 101 (2011)
8. Margaritondo G *Riv. Nuovo Cimento* **40** 411 (2017)
9. Bordovitsyn V A (Ed.) *Synchrotron Radiation Theory and Its Development in Memory of I.M. Ternov* (World Scientific Series on Synchrotron Radiation Techniques and Applications, Vol. 5) (Singapore: World Scientific, 1999)
10. Margaritondo G, in *Synchrotron Radiation. Basics, Methods and Applications* (Eds S Mobilio, F Boscherini, C Meneghini) (Berlin: Springer, 2015) p. 29
11. Placzek W et al. *Acta Phys. Pol. B* **50** 1191 (2019)
12. Saldin E L, Schneidmiller E A, Yurkov M V *The Physics of Free Electron Lasers* (Berlin: Springer, 2000)
13. Bonifacio R, Pellegrini C, Narducci L *Opt. Commun.* **50** 373 (1984)
14. Nakao N et al. *Nucl. Instrum. Meth. Phys. Res. A* **407** 374 (1998)
15. Sharma G, Mishra G, Gehlot M *JINST* **9** T01002 (2014)
16. Bazouband F, Maraghechi B *J. Plasma Phys.* **81** 905810305 (2015)
17. Asakawa M et al. *Nucl. Instrum. Meth. Phys. Res. A* **318** 538 (1992)
18. Asakawa M et al. *Nucl. Instrum. Meth. Phys. Res. A* **358** 399 (1995)
19. Asakawa M et al. *Nucl. Instrum. Meth. Phys. Res. A* **375** 416 (1996)
20. Iracane D, Bamas P *Phys. Rev. Lett.* **67** 3086 (1991)
21. Halbach K *J. Phys. Colloques* **44** C1-211 (1983)
22. Halbach K *J. Appl. Phys.* **57** 3605 (1985)
23. Prakash B et al. *Optik* **127** 1639 (2016)
24. Huse V et al. *Chin. Phys. Lett.* **31** 034101 (2014)
25. Lee K et al. *Nucl. Instrum. Meth. Phys. Res. A* **776** 27 (2015)
26. Jeevakhan H, Mishra G *Nucl. Instrum. Meth. Phys. Res. A* **656** 101 (2011)
27. Gupta V, Mishra G *Nucl. Instrum. Meth. Phys. Res. A* **574** 150 (2007)
28. Gupta V, Mishra G *Nucl. Instrum. Meth. Phys. Res. A* **556** 350 (2006)
29. Yang Y, Ding W *Phys. Plasmas* **5** 782 (1998)
30. Schmidt T et al., in *Proc. of the 36th Intern. Free Electron Laser Conf., FEL 2014, Basel, Switzerland, 25–29 August 2014* (Editorial Board: J Chrin, S Reiche, V R W Schaa) (Basel: JACoW, 2015) p. 116; http://accelconf.web.cern.ch/AccelConf/FEL2014/papers/mop043.pdf
31. Temnykh A B *Phys. Rev. ST Accel. Beams* **11** 120702 (2008)
32. Nuhn H-D et al., in *Proc. of the 37th Intern. Free Electron Laser Conf., FEL 2015, Daejeon, Korea, 23–28 August 2015* (Editorial Board: H S Kang, D-E Kim, V R W Schaa) (Daejeon: JACoW, 2015) p. 757; http://accelconf.web.cern.ch/FEL2015/papers/wed01.pdf
33. Henderson J R et al. *New J. Phys.* **18** 062003 (2016)
34. Emma P, in *Proc. of the 23rd Particle Accelerator Conf. 4–8 May 2009, Vancouver, British Columbia, Canada* (Vancouver: TRIUMF, 2010) p. 3115; http://accelconf.web.cern.ch/PAC2009/papers/th3pbi01.pdf
35. Emma P et al. *Nat. Photon.* **4** 641 (2010)
36. Ratner D et al. *Phys. Rev. ST Accel. Beams* **14** 060701 (2011)
37. Milton S V et al. *Science* **292** 2037 (2001)
38. Biedron S G et al. *Nucl. Instrum. Meth. Phys. Res. A* **483** 94 (2002)
39. Alferov D F, Bashmakov Yu A, Bessonov E G *Sov. Phys. Tech. Phys.* **18** 1336 (1974); *Zh. Tekh. Fiz.* **43** 2126 (1973)
40. Alferov D F, Bashmakov Yu A, Cherenkov P A *Sov. Phys. Usp.* **32** 200 (1989); *Usp. Fiz. Nauk* **157** 389 (1989)
41. Bagrov V G et al. *Teoriya Izlucheniya Relyativistskikh Chastits* (Theory of Radiation of Relativistic Particles) (Ed. V A Bordovitsyn) (Moscow: Fizmatlit, 2002)
42. Bagrov V G, Ternov I M, Kholomai B V *Izluchenie Relyativistskikh Elektronov v Prodol'nom Periodicheskom Elektricheskom Pole Kris-*

talla (Radiation of Relativistic Electrons in a Longitudinal Periodic Electric Field of a Crystal) (Tomsk: TF SO AN SSSR, 1987)
43. Dattoli G, Mikhailin V V, Ottaviani P L, Zhukovsky K V *J. Appl. Phys.* **100** 084507 (2006)
44. Vinokurov N A, Levichev E B *Phys. Usp.* **58** 850 (2015); *Usp. Fiz. Nauk* **185** 917 (2015)
45. Bessonov E G "K teorii istochnikov ondulyatornogo izlucheniya" ("On the theory of undulator radiation sources"), Preprint No. 18 (Moscow: Lebedev Physical Institute, USSR Academy of Sciences, 1982)
46. Alekseev V I, Bessonov E G, in *Trudy VI Vsesoyuznogo Soveshchaniya po Ispol'zovaniyu Sinkhrotronnogo Izlucheniya 'SI–84'* (Proc. of the 6th All-Union Conf. on the Use of Synchrotron Radiation 'SR-84') (Novosibirsk: IYaF SO AN SSSR, 1985) p. 92
47. Cherenkov P A (Exec. Ed.) *Ondulyatornoe Izluchenie, Lazery na Svobodnykh Elektronakh* (Undulator Radiation and Free-Electron Lasers) (Trudy FIAN, Vol. 214) (Moscow: Nauka, 1993); http://proceedings.lebedev.ru/0214-1993/
48. Bessonov E G *Nucl. Instrum. Meth. Phys. Res. A* **282** 405 (1989)
49. Alekseev V I, Bessonov E G *Nucl. Instrum. Meth. Phys. Res. A* **308** 140 (1991)
50. Kalitenko A M, Zhukovskii K V *J. Exp. Theor. Phys.* **130** 327 (2020); *Zh. Eksp. Teor. Fiz.* **157** 394 (2020)
51. Zhukovsky K *Results Phys.* **13** 102248 (2019)
52. Zhukovsky K *J. Synchrotron Rad.* **26** 1481 (2019)
53. Jeevakhan H, Mishra G *Opt. Commun.* **335** 126 (2015)
54. Zhukovsky K *J. Electromagn. Waves Appl.* **28** 1869 (2014)
55. Zhukovsky K V *Prog. Electromagn. Res. B* **59** 245 (2014)
56. Gould H W, Hopper A T *Duke Math. J.* **29** 51 (1962)
57. Dattoli G, Renieri A, Torre A *Lectures on the Free Electron Laser Theory and Related Topics* (Singapore: World Scientific, 1993)
58. Dattoli G *J. Appl. Phys.* **84** 2393 (1998)
59. Dattoli G, Ottaviani P L *Opt. Commun.* **204** 283 (2002)
60. Dattoli G, Ottaviani P L, Pagnutti S "Booklet for FEL design: a collection of practical formulae", ENEA Report RT/2007/40/FIM (2007)
61. Inoue I et al. *Nat. Photon.* **13** 319 (2019)
62. Zhukovsky K *Results Phys.* **19** 103361 (2020)
63. Zhukovsky K *Symmetry* **12** 1258 (2020)
64. Zhukovsky K *J. Synchrotron Rad.* **27** 1648 (2020)